Layer and interface structural changes in $Co_{0.6}Fe_{0.2}B_{0.2}/AlO_x$ multilayers on annealing

A. T. G. Pym,[1,a)] M. Rührig,[2] and B. K. Tanner[1,b)]
[1]*Department of Physics, Durham University, South Road, Durham DH1 3LE, United Kingdom*
[2]*Siemens AG, Corporate Technology MM1, 91502 Erlangen, Germany*

(Received 19 November 2009; accepted 15 February 2010; published online 7 May 2010)

Sputtered multilayers of $Co_{0.6}Fe_{0.2}B_{0.2}$ and AlO_x have been measured using grazing incidence x-ray scattering to determine the changes in layer and interface structure during *in situ* annealing. We confirm our earlier deduction of a sharpening of the interfaces on annealing up to 400 °C. This sharpening arises from reduction in chemical intermixing, not from change in topological roughness and provides an explanation for the enhanced tunneling magnetoresistance. The annealing is shown to result in a decrease in $Co_{0.6}Fe_{0.2}B_{0.2}$ mean layer thickness and increase in the layer density. There is a commensurate increase in AlO_x mean layer thickness while at the same time there is a reduction in the layer density. The increase in thickness could explain the corresponding increase observed in the resistance-area product. © *2010 American Institute of Physics*. [doi:10.1063/1.3366707]

I. INTRODUCTION

In magnetic tunnel junctions (MTJs), where electrons tunnel through a nanometer-scale insulating barrier between ferromagnetic electrodes, there is a continuing quest to increase the fractional change in the junction resistance (called the tunneling magnetoresistance or TMR) when the magnetization of the electrodes is switched from parallel to antiparallel. Despite the large amount of work in progress on MTJs with MgO barriers[1] and reports of TMRs as high as 230%,[2] the first MTJs into production, for example in magnetic random acess memory and automobile sensors, have alumina barriers and amorphous CoFeB electrodes. Although 70% TMR at room temperature has been claimed,[3] devices for which production is reliable have TMR typically 40%.

The spin polarization required for TMR operation has been shown to be highly influenced by the electronic and structural nature of the interfaces[4] and thus it is crucial for the optimization of device performance that the interface growth be under precise control. It is believed that the addition of boron improves the perfection of the interfaces by creating an amorphous structure that does not replicate the crystalline grain growth from the layer underneath.

A low temperature annealing stage in the manufacturing process is regularly used to enhance the TMR of MTJ devices.[5] We have previously reported experiments showing that in the annealing process, used to maximize the TMR without pushing the resistance-area product unacceptably high,[6] the interface between the alumina barrier and bottom CoFeB electrode reduces in width, there being no change in topological roughness.[7] As the grazing incidence x-ray scattering experiments were conducted on partial device structures, this conclusion of chemical sharpening arose from detailed modeling of complex reflectivity profiles. In this paper, we report similar *in situ* annealing experiments on simplified periodic multilayer structures. Despite the risk that the interface perfection may degrade as the repeated number of layers increases, the modeling and interpretation of the x-ray reflectivity and diffuse scatter can be achieved with much greater confidence. In particular, Bragg sheets appear in reciprocal space associated very specifically with the conformal roughness of the interfaces.

II. EXPERIMENTAL DETAILS

Samples were prepared in Erlangen by magnetron sputtering on plasma-etched, thermally oxidized Si wafers. The nominal layer structures were $[Co_{0.6}Fe_{0.2}B_{0.2}(3\ nm)/AlO_x(1.2\ nm)]_{x5}$. Base pressure in the sputter system is in the range of 4×10^{-8} mbar and the Ar sputter gas pressure was set to 5 μbar. Sputtering of the magnetic and dielectric layers was performed in dedicated sputter chambers, to prevent cross-contamination. Before deposition of the layer stack the substrate was precleaned by plasma etching for 15 min. Whereas each of the 3 nm thick CoFeB layers is made out of a multiple of 20 sublayers by subsequently rotating the substrate across the target (2 rpm), the 1.2 nm aluminum layer is deposited in a single run (3.5 rpm). Afterwards the aluminum is oxidized in a plasma process using $Ar/O_2(5\%)$ sputter gas at a pressure of 10 μbar. This process of sputter-etching, where the argon in the plasma etches into the aluminum and the aluminum is oxidized at the same time[8,9] results in the stochiometry being governed by the ratio of argon to oxygen in the plasma, and the length of time the plasma is applied to the sample. As the stoichiometry is not exactly Al_2O_3, the material is referred to as AlO_x. The thickness of the aluminum oxide is typically 30% more than that of the Al originally deposited.[10] An increase in thickness of approximately two has been previously observed following glow discharge oxidation.[11]

High resolution grazing incidence x-ray scattering experiments were performed at the, now closed, SRS synchrotron radiation source at Daresbury Laboratory. *In situ* reflectivity measurements were made during annealing in a high

a)Present address: Kromek, NETPark, Thomas Wright Way, Sedgefield, County Durham, TS21 3FD, U.K.
b)Electronic mail: b.k.tanner@dur.ac.uk.

 © 2010 American Institute of Physics

Downloaded 09 Oct 2012 to 129.234.252.65. Redistribution subject to AIP license or copyright; see http://jap.aip.org/about/rights_and_permissions

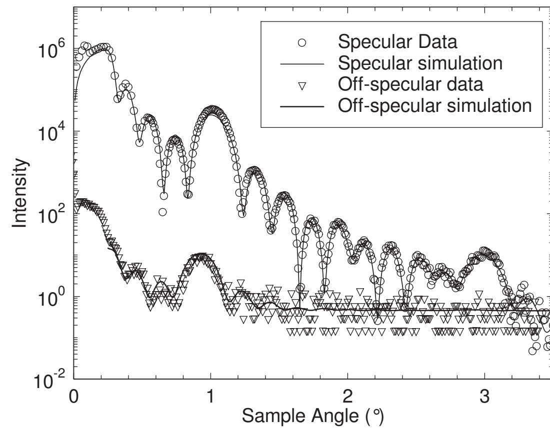

FIG. 1. Specular (circles) and off-specular (triangles) scatter at room tempertaure from the as-grown structure. The off-specular scatter is taken as a scan of detector and sample in the ratio of 2:1 with the sample displaced by $-0.1°$ from the specular condition. Solid lines are best-fit simulations using the parameters in Table I and an in-plane correlation length of 100 ± 20 nm, out-of-plane correlation length of 200 ± 100 nm, fractal parameter 0.7 ± 0.2, and rms topological roughness of 0.055 nm.

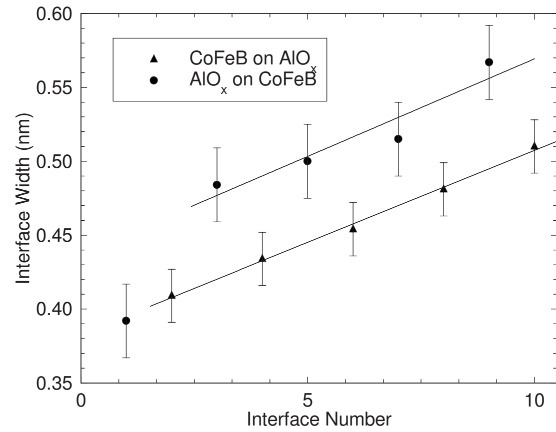

FIG. 2. Interface width as a function of repeat number.

purity argon atmosphere slightly above atmospheric pressure. The chamber was carefully flushed through with argon before measurements were taken. Heating was by the induction furnace on station 2.3 using alignment and data collection techniques that are standard to all such measurements. To maximize the intensity from the bending magnet, a wavelength λ of 0.13 nm was selected from the channel-cut 111 Si crystal monochromator. Specular and diffuse x-ray scatter was fitted to model structures using the BEDE REFS software package.[12]

III. RESULTS

A. As-grown structures

An example of the specular and off-specular scatter from a typical sample is shown in Fig. 1. Good agreement between experimental and simulated curves could be obtained only when the interface width was assumed to increase systematically through the stack. The parameters used in Fig. 1 are given in Table I, together with the statistical precision on the layer thickness and interface width values. (We note that the electron density of the Si substrate and the thermal oxide layer is too small to detect any effect of this interface in the reflectivity curves and the thickness of the oxide is taken as infinite.) The variation in the fitted value for layer thickness through the multilayer is greater than the statistical precision in the fit. This is probably a result of cross-correlation of parameters when searching for the global minimum in the difference between simulated and experimental curves. There is no systematic variation in thickness through the stack.

TABLE I. Layer thickness, fractional density, and interface width.

Layer	Material	Thickness (nm)	Density of bulk (%)	Interface width (nm)
10	Al_2O_3	2.029 ± 0.048	80.0 ± 6.1	0.510 ± 0.016
9	$Co_{0.6}Fe_{0.2}B_{0.2}$	1.783 ± 0.038	84.2 ± 2.3	0.567 ± 0.028
8	Al_2O_3	1.704 ± 0.024	85.0 ± 5.0	0.481 ± 0.021
7	$Co_{0.6}Fe_{0.2}B_{0.2}$	1.796 ± 0.040	85.0 ± 2.7	0.515 ± 0.023
6	Al_2O_3	1.943 ± 0.026	80.0 ± 5.2	0.454 ± 0.015
5	$Co_{0.6}Fe_{0.2}B_{0.2}$	1.871 ± 0.023	82.7 ± 2.9	0.500 ± 0.020
4	Al_2O_3	1.851 ± 0.033	80.7 ± 6.1	0.434 ± 0.015
3	$Co_{0.6}Fe_{0.2}B_{0.2}$	1.860 ± 0.025	80.0 ± 4.0	0.484 ± 0.021
2	Al_2O_3	1.836 ± 0.026	85.0 ± 9.9	0.409 ± 0.02
1	$Co_{0.6}Fe_{0.2}B_{0.2}$	1.860 ± 0.024	81.2 ± 7.8	0.392 ± 0.026
Substrate	SiO_2	∞	98.8 ± 30.3	0.332 ± 0.016

Careful fitting of the specular reflectivity to the data revealed that the interface width of the $Co_{0.6}Fe_{0.2}B_{0.2}$ on Al_2O_3 interfaces was lower than that of the Al_2O_3 on $Co_{0.6}Fe_{0.2}B_{0.2}$ interfaces, both interface widths increasing linearly with repeat number at the almost the same rate (Fig. 2). The topological roughness and interdiffusion profile cannot be separated from measurement of the specular scatter alone, as the electron density profile is sampled only in the direction normal to the surface. However, measurement of the off-specular scatter enables the two effects to be distinguished. We observed that the off-specular scatter is low. By fitting simulations from a model structure to the data (Fig. 1), we found that the best-fit topological roughness was 0.055 nm and thus responsible for only about 10% of the interface width. We note that the increase in the total interface width with multilayer repeat (Fig. 2) is greater than the topological roughness. As the intermixing width and topological roughness add in quadrature, the observed increase in total interface width must therefore arise from increased chemical intermixing at the interfaces, not an increase in topological roughness.

The roughness amplitude is determined by the amount of diffuse scatter; the distribution of diffuse scatter is determined by the in-plane roughness parameters. Simulation of the rocking curve with the parameters used to fit the off-specular scan of Fig. 1 shows an excellent fit to the experimental data (Fig. 3). The fractal parameter of 0.7 corresponds to a fractal dimension of 2.3 and the in-plane correlation length of 100 nm of these amorphous systems is long compared, for example, with low repeat number multilayers of polycrystalline Co/Pd (Ref. 13) or ultra-hugh vacuum evaporated Co/Cr trilayers.[14] We also note that the out-of-plane correlation length of the roughness is long com-

Downloaded 09 Oct 2012 to 129.234.252.65. Redistribution subject to AIP license or copyright; see http://jap.aip.org/about/rights_and_permissions

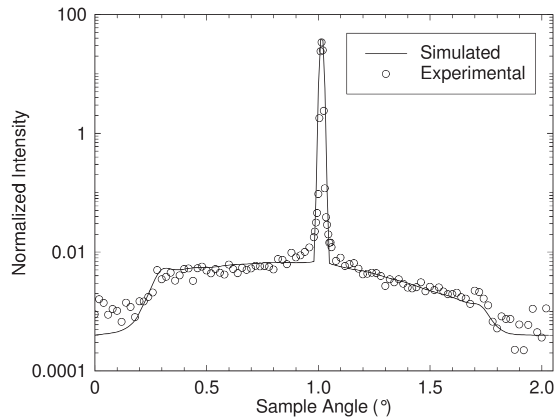

FIG. 3. Experimental and simulated rocking curve (sample scan at fixed scattering angle).

pared with the total multilayer stack thickness. To a good approximation, the roughness is conformal throughout the stack.

B. Effects of annealing

On annealing, the most noticeable change was in the height of the third order Bragg peak, which increased systematically with temperature (Fig. 4). With the assumption of a linear variation in interface width, we were able to obtain similar quality fits to that at room temperature between simulation and experiment for all temperatures during the annealing process (Fig. 5). By such careful fitting of the whole reflectivity profiles, we have determined the average width of both $Co_{0.6}Fe_{0.2}B_{0.2}$ on Al_2O_3 interfaces and Al_2O_3 on $Co_{0.6}Fe_{0.2}B_{0.2}$ interfaces as a function of annealing temperature. Both fell linearly with temperature (Fig. 6) though at different rates for the two types of interface. Measurement of the diffuse scatter showed that the topological roughness of the multilayer interfaces remained of constant amplitude and no changes were found for the in-plane length scale of the roughness. The reduction in interface width therefore arises from a sharpening of the chemical profile across the interfaces. This is consistent with our observations of the behavior of $Co_{0.6}Fe_{0.2}B_{0.2}/Al_2O_3$ interfaces in the more complex MTJ structures.[7]

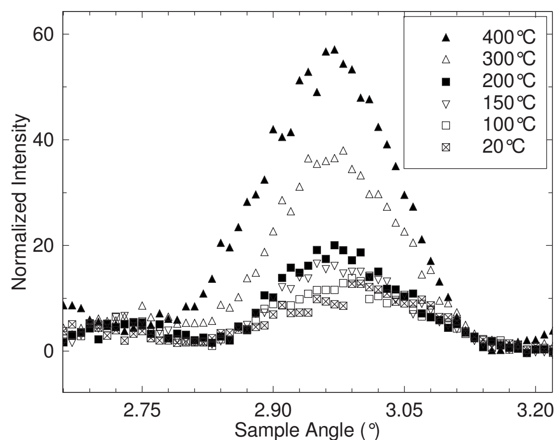

FIG. 4. Variation in height of third order multilayer Bragg peak for various temperature values.

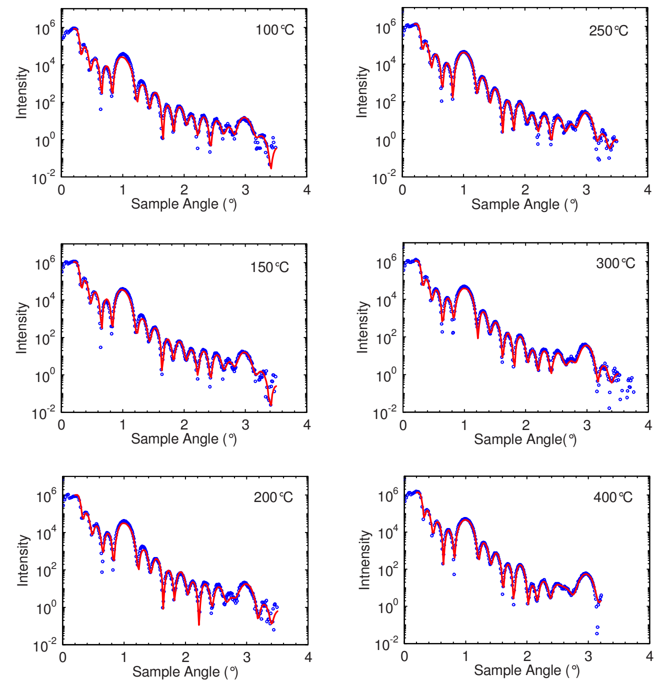

FIG. 5. (Color online) Best fits between simulated (solid line) and experimental (points) specular reflectivity at different annealing temperatures.

Up to a temperature of approximately 250 °C, there was no significant change in the mean thickness of the layers outside of the measurement precision, but above this temperature, the $Co_{0.6}Fe_{0.2}B_{0.2}$ average layer thickness decreased, while the average Al_2O_3 thickness correspondingly increased (Fig. 7). At the same time, the average $Co_{0.6}Fe_{0.2}B_{0.2}$ layer density increased by about 3%, while the average density of the Al_2O_3 layers showed a small decrease in about 1% (Fig. 8). While these values are not outside of the errors bars associated with the fitting procedure, there is, in both cases, an evident systematic trend in best-fit values.

IV. DISCUSSION

The diffuse x-ray scatter measurements confirm and quantify transmission electron microscopy measurements of

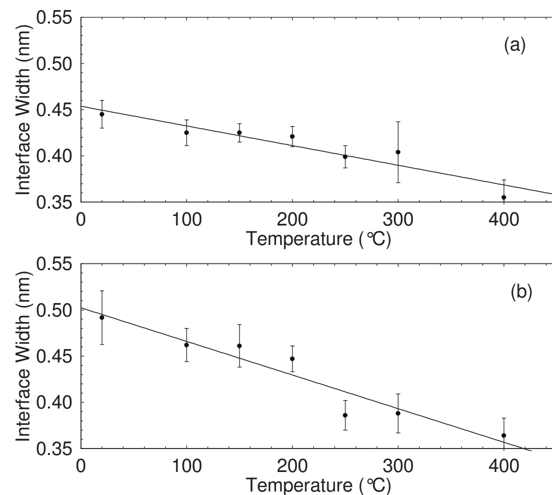

FIG. 6. Average interface width as a function of annealing temperature (a) $Co_{0.6}Fe_{0.2}B_{0.2}$ on Al_2O_3 and (b) Al_2O_3 on $Co_{0.6}Fe_{0.2}B_{0.2}$.

Downloaded 09 Oct 2012 to 129.234.252.65. Redistribution subject to AIP license or copyright; see http://jap.aip.org/about/rights_and_permissions

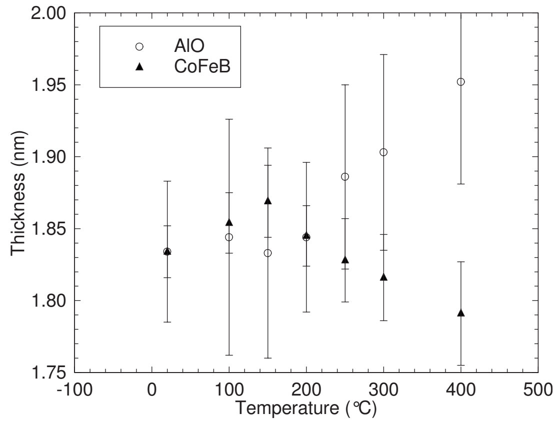

FIG. 7. Mean thickness of $Co_{0.6}Fe_{0.2}B_{0.2}$ and AlO_x layers as a function of annealing temperature.

the low value of the roughness amplitude in the $Co_{0.6}Fe_{0.2}B_{0.2}/AlO_x$ system.[15] It is generally accepted that this arises because of the absence of grains and the associated boundaries in these amorphous materials. A new observation is that the interface width increases with multilayer repeat, while there is no substantial increase in the topological roughness. All models of film growth predict an increase in roughness amplitude with increasing film thickness, the scaling exponent depending on the growth mechanism,[16] and our own simulations of multilayer growth using both ballistic and random deposition with surface relaxation models confirm this behavior.[17] However, the constancy of topological roughness with layer number in our best-fit simulation does not invalidate this description, as the experiment is ill-conditioned to extract these data. What is clear, nevertheless, is that the absolute value of the topological interface roughness is small compared with the total interface width and thus no gradient in topological roughness can account for the increase in total interface width. The reason for this increase in chemical intermixing with repeat number is not immediately obvious but could possibly arise from transfer of material through pinholes, which are known to exist in alumina tunnel barriers of this thickness.[18] Such a mechanism could account for the low value of the interface width, apparent in Fig. 2, between the first AlO_x layer and the first CoFeB layer compared with the subsequent AlO_x on CoFeB interfaces. The first AlO_x layer will have been deposited on a pinhole-free CoFeB layer, there thus being less material transport and a lower interface width. The amorphous nature of the films probably lies behind the almost two-dimensional nature of the interface, there being significantly less high frequency components to the in-plane roughness than in polycrystalline films.

Interface widths in the multilayer structures are very close to those previously measured in MTJ structures containing only a single alumina barrier and additional materials in the stack.[7] The decrease in interface width with annealing temperature is also very similar to the values deduced previously by a reverse modeling of a single feature in the complex reflectivity profile of the MTJ structure.[7] There is no doubt that the interface intermixing does reduce substantially during the annealing sequence. We observed some time ago that the width of the interface between Co and Al reduces when the Al is oxidised,[19] implying that the chemical potential is reduced by migration of the Al to form the oxide. It appears that this process is not complete and that on annealing there is additional movement of atoms, probably of Al to move the oxide composition closer to stochiometry. Such a presumption is consistent with the increase in thickness of the alumina barrier with annealing temperature (Fig. 7).

Sharpening of the interface could be the structural change responsible for the increased TMR on annealing $Co_{0.6}Fe_{0.2}B_{0.2}/AlO_x$ MTJs.[6,15] Calculation of the spin-dependent tunneling in epitaxial MgO/Fe junctions[20] reveals that interface disorder significantly reduces the TMR and by implication, reduction in interface intermixing width should also enhance the spin coherence in the amorphous system. However, associated with the increased TMR on annealing is also a rise in the resistance-area product. As the tunneling resistance is an exponential function of barrier thickness, a small change in barrier width can result in a substantial change in resistance. The thickness of an MTJ barrier is chosen to optimize the conflicting requirement of high TMR and minimal resistance, required to reduce noise. There is a small increase in alumina barrier thickness at the higher annealing temperatures which may be responsible for the increase in resistance-area product observed above about 300 °C.[6]

The reduction in alumina barrier density may be associated both with a change in stochiometry, from the reduction in interface width, and the conservation of material necessary upon increase in the barrier thickness. Increase in density of the $Co_{0.6}Fe_{0.2}B_{0.2}$ layers is consistent with conservation of material upon decrease in $Co_{0.6}Fe_{0.2}B_{0.2}$ layer thickness.

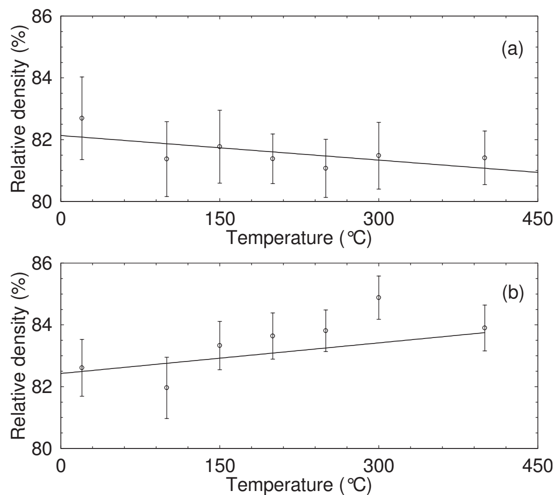

FIG. 8. Average layer density of the (a) AlO_x and (b) $Co_{0.6}Fe_{0.2}B_{0.2}$ layers as a function of annealing temperature.

V. CONCLUSIONS

Grazing incidence x-ray scattering measurements have confirmed that annealing of $Co_{0.6}Fe_{0.2}B_{0.2}$ and AlO_x films results in reduction in the chemical intermixing at the interface, the values of the changes being consistent with earlier, less directly interpretable, measurements. This reduction provides a possible mechanism for the well established increase

Downloaded 09 Oct 2012 to 129.234.252.65. Redistribution subject to AIP license or copyright; see http://jap.aip.org/about/rights_and_permissions

in TMR obtained when tunnel junctions are annealed. The increase in resistance-area product on annealing may be related to the observed increase in thickness of the alumina layers.

ACKNOWLEDGMENTS

Financial support from the UK Engineering and Physical Sciences Research Council and through the European Community's Marie Curie actions (Research Training Networks) under Contract No. MRTN-CT-2003-504462, ULTRASMOOTH.

[1] S. Yuasa, T. Nagahama, A. Fukushima, Y. Suzuki, and K. Ando Nature (London) **3**, 868 (2004).
[2] D. D. Djayaprawira, K. Tsunekawa, M. Nagai, H. Maehara, S. Yamagata, N. Watanabe, S. Yuasa, Y. Suzuki, and K. Ando, Appl. Phys. Lett. **86**, 092502 (2005).
[3] D. X. Wang, C. Nordman, J. M. Daughton, Z. H. Qian, and J. Fink, IEEE Trans. Magn. **40**, 2269 (2004).
[4] E. Y. Tsymbal and K. D. Belashchenko, J. Appl. Phys. **97**, 10C910 (2005).
[5] R. C. Sousa, V. Soares, P. P. Freitas, A. Kling, M. F. Da Silva, and J. C. Soares, Appl. Phys. Lett. **73**, 3288 (1998).
[6] T. Dimopoulos, G. Gieres, J. Wecker, N. Weise, and M. D. Sacher, J. Appl. Phys. **96**, 6382 (2004).
[7] A. T. G. Pym, A. Lamperti, B. K. Tanner, T. Dimopoulos, M. Rührig, and J. Wecker, Appl. Phys. Lett. **88**, 162505 (2006).
[8] J. Nassar, M. Hehn, A. Vaures, F. Petroff, and A. Fert, Appl. Phys. Lett. **73**, 698 (1998).
[9] J. H. Greiner, J. Appl. Phys. **42**, 5151 (1971).
[10] T. Dimopoulos, V. Da Costa, C. Tiusan, K. Ounadjela, and H. A. M. Van den Berg, J. Appl. Phys. **89**, 7371 (2001).
[11] J. D. R. Buchanan, T. P. A. Hase, B. K. Tanner, N. D. Hughes, and R. J. Hicken, Appl. Phys. Lett. **81**, 751 (2002).
[12] M. J. Wormington, C. Panaccione, K. M. Matney, and D. K. Bowen, Philos. Trans. R. Soc. London, Ser. A **357**, 2827 (1999) the software is now available from Jordan Valley Semiconductor.
[13] A. T. G. Pym, A. S. H. Rozatian, C. H. Marrows, S. D. Brown, L. Bouchenoire, T. P. A. Hase, and B. K. Tanner, J. Phys. D **38**, A190 (2005).
[14] T. P. A. Hase, E. M. Ho, J.-J. Frejo, S. M. Thompson, A. K. Petford-Long, and B. K. Tanner, J. Phys. D **36**, A231 (2003).
[15] F. F. Li, R. Sharif, L. X. Jiang, X. Q. Zhang, X. F. Han, Y. Wang, and Z. Zhang, J. Appl. Phys. **98**, 113710 (2005).
[16] A.-L. Barabás and H. E. Stanley, *Fractal Concepts in Surface Growth*, (Cambridge University Press, Cambridge, 1995) p. 366.
[17] A. T. G. Pym, Ph.D. thesis, Durham University, 2008.
[18] A. Cerezo, A. K. Petford-Long, D. J. Larson, S. Pinisoontorn, and E. W. Singleton, J. Mater. Sci. **41**, 7843 (2006).
[19] J. D. R. Buchanan, T. P. A. Hase, B. K. Tanner, P. J. Chen, L. Gan, C. J. Powell, and W. F. Egelhoff, J. Appl. Phys. **93**, 8044 (2003).
[20] J. Mathon and A. Umerski, Phys. Rev. B **74**, 140404 (2006).

Downloaded 09 Oct 2012 to 129.234.252.65. Redistribution subject to AIP license or copyright; see http://jap.aip.org/about/rights_and_permissions